Nanoscale

RSCPublishing

REVIEW

View Article Online
View Journal | View Issue

Cite this: *Nanoscale*, 2013, **5**, 6627

Efficient photon management with nanostructures for photovoltaics

Bo Hua, Qingfeng Lin, Qianpeng Zhang and Zhiyong Fan*

Received 6th March 2013
Accepted 14th April 2013

DOI: 10.1039/c3nr01152f

www.rsc.org/nanoscale

Efficient photon management schemes are crucial for improving the energy conversion efficiency of photovoltaic devices; they can lead potentially to reduced material usage and cost for these devices. In this review, photon trapping mechanisms are discussed briefly in the beginning, followed by a summary of recent progress on a number of major categories of nanostructures with intriguing photon management properties. Specifically, nanostructures including nanowires, nanopillars, nanopyramids, nanocones, nanospikes, and so forth, have been reviewed comprehensively with materials including Si, Ge, CdS, CIGS, ZnO, *etc.* It is found that these materials with diverse configurations have tunable photon management properties, namely, optical reflectance, transmittance and absorption. Investigations on these nanostructures have not only shed light on the fundamental interplay between photons and materials at the nanometer scale, but also suggested a potential pathway for a new generation of photovoltaic devices.

1 Introduction

Although solar energy is by far the most abundant clean-energy resource, and photovoltaic (PV) devices can directly convert solar electromagnetic radiation to electricity for convenient transportation and utilization, large scale deployment of solar PV panels to account for a significant portion of global generation has not been feasible, primarily due to twofold reasons. One is that the energy density of solar irradiance ($\sim$1 kW m^{-2}) on the earth's surface is relatively low, so is the energy conversion efficiency of the dominant PV technology, *i.e.* $\sim$15% for a crystalline Si panel. The other is that the cost of the current PV technologies is not as competitive as that of the conventional energy sources.[1] To address these two issues, improving PV conversion efficiency is crucial, as well as reducing the material and module manufacturing cost. In recent years, enormous efforts have been invested in developing a new generation of low cost PV materials and novel device structures.[2–4] In addition, the fundamental interplay between photons and materials/structures down to the nanometer scale has been revisited for more efficient light harvesting. Particularly, an assortment of nanostructures has been fabricated with various techniques, and their electrical and optical properties have been explored systematically.[5–14]

Department of Electronic & Computer Engineering, Hong Kong University of Science & Technology (HKUST), Hong Kong SAR, China. E-mail: eezfan@ust.hk

Bo Hua received his BS degree in Optical Science and Engineering from Fudan University, Shanghai, China in 2011. He is now a postgraduate student in the Department of Electronic and Computer Engineering of Hong Kong University of Science and Technology. His current research interests include simulation and fabrication of nanophotonics based on nanostructures, for application in photovoltaics and other optoelectronics.

Qingfeng Lin is a PhD student in the Department of Electronic and Computer Engineering in the Hong Kong University of Science and Technology. He received his BS degree in Electronic Science and Technology from the University of Science and Technology of China. His current research interests focus on the fabrication of nanostructures with self-organized approaches, and their applications on nanophotonics and nanoelectronics.

Notably, it has been discovered that organizing these nanostructures into random or regular arrays leads to their unique photon management properties, namely, tunable optical reflectance, transmittance and absorption.[15–22] More importantly, properly designed nanophotonic structures have shown the potency to demonstrate light absorption exceeding conventional limits.[23] These achievements have paved the way for developing a new generation of PV technologies and thus will have profound impact. In this paper, we aim to provide a comprehensive review of recent progress on several major categories of nanostructures with intriguing photon management properties. These nanostructures include nanowires (NWs), nanopillars (NPLs), nanopyramids (NPMs), nanocones (NCNs), nanospikes (NSP), nanowells (NWLs), and nanoparticles (NPs). We will begin with a brief review of photon trapping mechanisms in materials which serves as a background for nanostructure photon management. Then, the fabrication and optical property investigations of the aforementioned nanostructures will be discussed in detail. Particularly, the different characteristics of these nanostructures will be emphasized, and optical design guidelines for efficient light harvesting will be presented. In the end, a summary will be provided with perspectives on future development of nanostructures for photon management and PV applications.

2 Light trapping theory and mechanisms

One of the traditional methods to reduce the reflection loss on the surface of a PV device and thus enhance the light absorption is to use an anti-reflection layer, including Si_3N_4, SiO_2, *etc.* The thickness of the anti-reflection layer is usually designed to a quarter of wavelength, making the phase difference of the incident light and reflected light half a wavelength, thus reflection is suppressed through destructive interference. However, it is obvious that a quarter wavelength anti-reflection layer works the best only for an individual wavelength. What's more, if the incident light is oblique, the anti-reflection effect will also be weakened due to change of the light travel path. Meanwhile, the fabrication process of an anti-reflection layer typically involves vacuum deposition equipment thus is usually not low-cost.

Random-texturization of the surface is another way to realize light trapping and absorption enhancement. By roughening the device surface on the micron scale, light will be scattered on the front surface of a PV device and then propagate into the light-absorber material in a random direction. With a back reflector on the bottom of the device, the optical path can be further prolonged, resulting in an absorption enhancement of up to $4n^2/\sin^2\theta$, where n is the refractive index of the material and θ is half of apex angle of the absorption cone.[23,24] This is known as Lambertian limit, or Yablonovitch limit.[25–29] For single

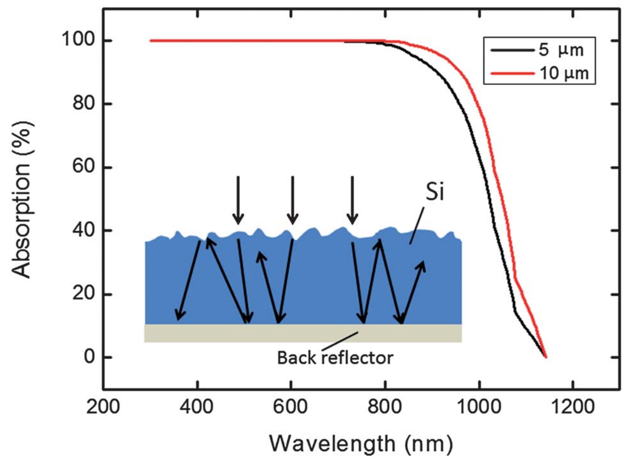

Fig. 1 Lambertian limit of 5 μm and 10 μm thick silicon thin films. Inset: schematic of light scattering in Si films with rough surface texturing and a back reflector.

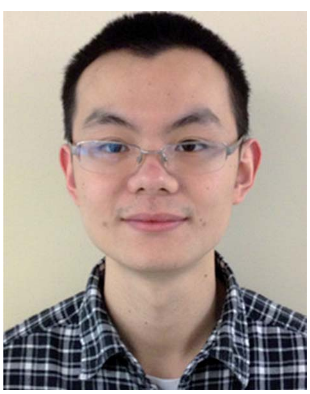

Qianpeng Zhang is a PhD student in the Department of Electronic and Computer Engineering in Hong Kong University of Science and Technology. He received his BEng degree from the School of Optical and Electronic Information in Huazhong University of Science and Technology in 2008. His current research interests focus on optical and electrical simulations of solar cells.

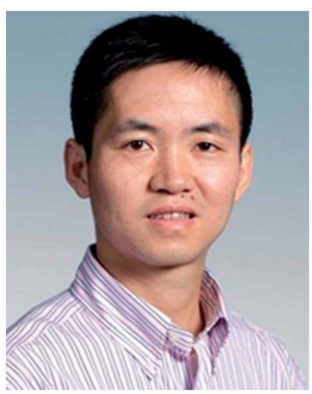

Zhiyong Fan received his BS and MS degrees in Physical Electronics from Fudan University, Shanghai, China, in 1998 and 2001. He received his PhD degree from the University of California, Irvine, in 2006 in Materials Science. From 2007 to 2010 he worked in the University of California, Berkeley, as a postdoctoral fellow in the department of Electrical Engineering and Computer Sciences, with a joint appointment with Lawrence Berkeley National Laboratory. In May 2010, he joined Hong Kong University of Science and Technology as an assistant professor. His research interests include engineering novel nanostructures with functional materials, for technological applications including energy conversation, electronics and sensors, etc.

crystalline silicon solar cells, n is about 3.5, thus the enhancement factor is about 50 considering the isotropic response with $\theta = 0$.[29] The Lambertian limit curves of 5 μm and 10 μm thick silicon layers are plotted in Fig. 1. It illustrates that almost 100% absorption is obtained in the wavelength range of 300–800 nm, while for longer wavelengths the absorption is relatively low due to lower absorption coefficient. Considering the high cost of crystalline PV materials nowadays, it is of great importance to find a structure that can absorb light with high efficiency while use less amount of material in the PV devices. On the other hand, it is worth noting that reduction of the material thickness could also result in less carrier-recombination as mentioned before.

The development of nanostructure fabrication techniques allows a further understanding of the interactions of photons with materials on the nanometer scale. With a material thickness of several microns or even several hundred nanometers, nanostructures could maintain a high optical absorption close to the Lambertian limit, or even exceed the Lambertian limit.[23,29] It was found that arrays of sub-wavelength nanostructures can realize a smooth or stepwise transition of effective refractive index from air to semiconductor materials.[30] The effective refractive index of a nanostructured film is defined as $n_{\text{eff}} = n \times \text{FR}$, where n is the refractive index of material and FR is the material filling ratio.[31] Specifically, for NW arrays with a uniform NW diameter, n_{eff} depends on the relationship between the NW diameter and pitch. While for multiple-diameter nanostructures or even gradually varied diameter nanostructures like NCNs, a smoother effective refractive index transition or even a continuous transition can be realized, thus the reflection can be reduced to a very small value.[31,32]

The wave nature of light enables more interesting interactions between photons and nanostructures. For example, NWs can act as dielectric resonators, so that light can be coupled into different transverse resonance leaky modes by controlling the diameter of NWs, thus the absorption spectrum can be engineered.[33,34] In fact, leaky mode resonances (LMR) can be supported by not only one-dimensional (1-D) nanowires, but also 2-dimensional planar films and zero-dimensional (0-D) nanoparticles.[34,35] What's more, spherical nanoshells can support whispering gallery modes, so that optical path of the coupled light can be enhanced significantly.[36] When nanostructures are organized into photonic crystals, some new and interesting properties appear such as a photonic band-gap. It has been shown that the optical absorption of solar cells can be improved *via* the photonic crystal effect.[37–41]

Recently, plasmonics have attracted increasing attention as well. This suggests that electromagnetic wave energy can be localized and guided into materials with metallic nanostructures.[42–44] In brief, the plasmonic light absorption enhancement can be implemented *via* three geometries, as shown in Fig. 2.[45] Firstly, metal nanoparticles can help scatter photons into devices, as shown in Fig. 2a. Secondly, metal nanoparticles can act as antennas to enhance the local electric field intensity (Fig. 2b), thus leading to enhanced absorption locally. Thirdly, surface plasmon polariton (SPP) modes can be excited at the interface of metal and dielectric materials, as shown in Fig. 2c. The SPP modes will propagate along the interface, and coupled electromagnetic waves can be absorbed by semiconductor materials, if well designed. In most plasmonic designs, noble metals like Ag and Au are chosen, while it is believed that for large scale applications, metals with an abundant reserve are better choices, *i.e.* Al, Cu, *etc.*[45]

In the sections below, light management with a variety of nanostructures will be introduced. The goal is to identify not only the mechanism of photon management with different structures, but also the rational design of nanostructures for optimal light absorption.

3 Photon management properties of various nanostructures

3.1 Nanowires and nanopillars

3.1.1 Nanowires (NWs). NWs and NPLs can both be categorized as quasi-one-dimensional materials, while NPLs normally refer to short and vertical standing NWs. In fact, NWs have been widely investigated and utilized for PV devices in the past few years, with various materials including Si[20,22,46–48] InAs,[49] InP,[50] ZnO,[51] *etc.* Nanostructure-based PV devices usually have large surface recombination rates compared to traditional Si solar cells and thin film solar cells. However, the carrier transport ability of NWs and NPLs can be superior compared to other nanostructures, especially nanoparticles. Law *et al.* calculated that the electron diffusivity for single ZnO NWs is 0.05–0.5 $\text{cm}^2\ \text{s}^{-1}$, which is hundreds of times larger than that of TiO_2 and ZnO nanoparticle films.[51] Generally, there are two types of p–n junction configurations, *i.e.* radial junctions and axial junctions.[52,53] Compared to axial junctions, the configuration of the radial (core–shell) junction can further enhance the carrier collection efficiency, as long as the radii of the NWs are much smaller than the minority diffusion length.[53–55] Nanowires can also be embedded into thin films to form junctions, which was also proven to be an efficient way to improve carrier collection efficiency.[6]

The photon management properties of NWs have been well studied.[19,34,35,48,50,56,57] Theoretical and experimental works have shown that arrays of semiconductor NWs with well-defined diameter, length, and pitch have tunable reflectance, transmittance, and absorption. Fig. 3a shows an SEM image of Si nanowire arrays on an Si wafer reported by Garnett and Yang.[46] The NW arrays were fabricated by deep reactive ion etching (DRIE) using a monolayer film of silica beads as a mask. The pitch and diameter of Si NWs can be controlled by silica beads, while the length is determined by etch time. Optical transmittance measurements showed that the absorption of Si thin films with NW arrays on the top is much higher than their planar counterpart with the same device thickness of about 8 μm, as shown in Fig. 3b. For the planar device, because the absorption coefficient of Si at long wavelengths is much lower than that at short wavelengths, the transmittance is high for 700 nm and longer wavelengths. The transmittance curve oscillates at this part due to the interference effect. Meanwhile, for a sample with NW arrays, the transmittance is lower than 10% from wavelengths of 400 nm to 1000 nm with a 2 μm thick

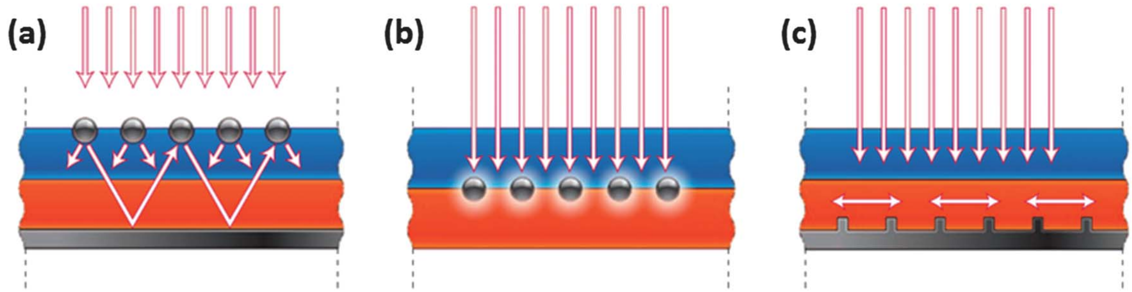

Fig. 2 Three schemes of the plasmonic effect. (a) Light is scattered by metal particles in a large angle, causing the increase of the effective optical path length. (b) The excitation of localized surface plasmons causes the enhancement of the local electric field. (c) Light is coupled by the surface plasmon polariton or photonic modes which can propagate along the interface. (Reprinted from ref. 45, Copyright 2010 Nature Publishing Group.)

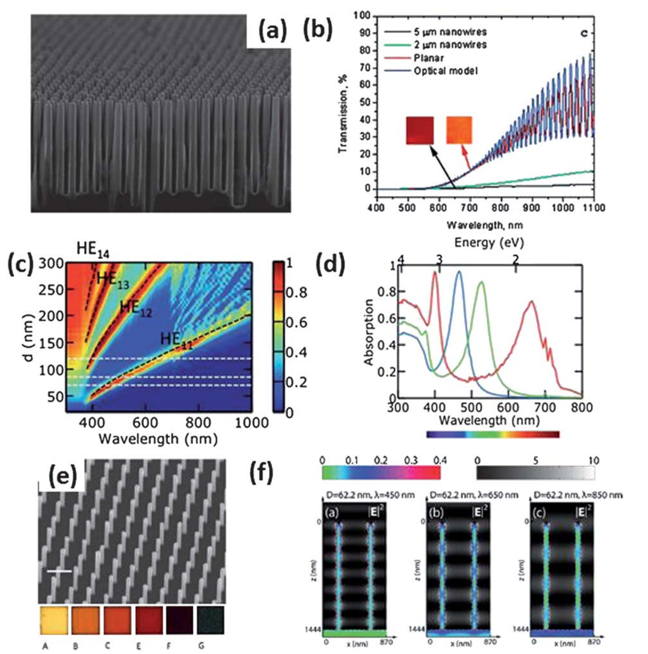

Fig. 3 (a) SEM picture of an ordered silicon NW radial p–n junction array solar cell. (b) Transmittance spectra of silicon window structures with 5 μm (black), 2 μm (green) long NWs and without NWs (orange), with the blue curve corresponding to the optical model result. The insets are backlit color images of samples. (Reprinted from ref. 46, Copyright 2010 American Chemical Society.) (c) 2-D contours of absorption as a function of NW diameter and wavelength for vertical Si NW arrays. The dashed line corresponds to curves in (d). (d) Absorption curves of NW arrays with a diameter of 70 nm, 85 nm, and 120 nm. (Reprinted from ref. 57, Copyright 2012 The Optical Society.) (e) 30-degree-tilted SEM picture of InAs NW arrays corresponding to sample A. Below are the color images of the different samples. (f) Electric field intensity square distributions of NW with 62.2 nm diameter at different wavelengths. (Reprinted from ref. 49, Copyright 2010 American Chemical Society.)

NWs layer. With an NW length of 5 μm, the transmittance is close to zero. Considering the fact that a sample with NW arrays has less material than a planar device, the light absorption performance of NW arrays is quite attractive.

In addition to photon absorption enhancement *via* scattering inside an NW array, it was found that even a single NW can demonstrate interesting photon management properties. Cao *et al.* showed that certain leaky mode resonances can occur in a single semiconductor NW, which can confine electromagnetic energy effectively.[33] Wang and Leu also calculated the leaky modes in silicon NW arrays.[57] They demonstrated that due to symmetry matching requirements, incident light on vertical NWs can only couple to HE_{1m} leaky modes, as shown in Fig. 3c. By varying the diameter of NWs, the wavelength associated with leaky modes and the resulting transverse resonance can be tuned. Accordingly, wavelength-selective absorption can be realized by controlling the diameter, as shown in Fig. 3d, which corresponds to the dashed line cross-sections in Fig. 3c. The blue, green, and red curves are responsible for 70 nm, 85 nm, and 120 nm diameter NWs, respectively. The leaky mode resonances are caused by the finite NW size and large refractive index contrast between the semiconductor nanowires and their surroundings, so this effect is applicable to other semiconductor materials, *i.e.* Ge, amorphous Si, CdTe, *etc.*[31,58] The above results are not only valuable for PV application, but also useful for other optoelectronic applications such as color-selective photodetectors.

Besides Si NWs, Wu *et al.* also reported that optical absorption of InAs NWs can be tuned by geometrical tuning.[49] Fig. 3e shows the SEM image of InAs NWs grown in a high vacuum chemical beam epitaxy (CBE) unit by using electron beam lithography (EBL) defined gold dots as seeds. With different diameter and length, the colors of NW sample array devices are different, which reveals their different optical reflection spectra. From the calculated electric field intensity distributions in Fig. 3f, the vertical resonance can be clearly observed. Since the absorption coefficient of InAs decreases with increase of wavelength, an optical absorption of 850 nm is not as strong as a 450 nm wavelength. With a proper choice of diameter, length, and pitch, InAs NWs can also absorb either much more or much less light than a thin film counterpart, akin to Si NWs.

3.1.2 Nanopillars (NPLs). Besides NWs, NPL arrays have been extensively and successfully fabricated for efficient photon management and solar energy conversion with materials including CdS, Ge, Si, InP, SiO_2, and so forth.[6,14,59–63] In fact, NPLs can be more advantageous than NWs for PV applications due to their smaller surface area and less surface recombination, which is the one of the major issues for nanostructured solar cells.[2,11] While for single-diameter NPLs (Fig. 4a), which are similar to NWs discussed above, it was found that the increase of the light absorptive material filling ratio leads to the increase of reflectance and the decrease of transmittance

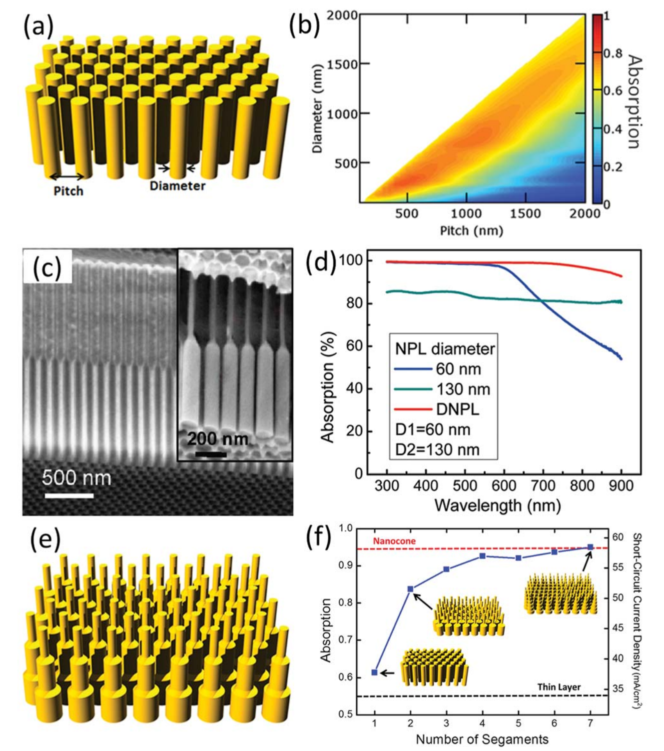

Fig. 4 (a) Schematic of hexagonal Ge NPL arrays with a single-diameter. (b) 2-D contour of broadband absorption of Ge single-diameter NPL arrays. (Reprinted from ref. 31, Copyright 2013.) (c) Cross-sectional SEM images of a blank AAM with dual-diameter pores and the Ge DNPLs (inset) after the growth. (d) Experimental absorption spectra of a DNPL array with $D_1 = 60$ nm and $D_2 = 130$ nm, and single-diameter NPL arrays with diameters of 60 and 130 nm. (Reprinted from ref. 16, Copyright 2010 American Chemical Society.) (e) Schematic of hexagonal Ge NPL arrays with multi-diameters. (f) Broadband-integrated absorption of 1000 nm pitch Ge MNPL arrays as a function of segment number. Dashed line represents the broadband-integrated absorption of 1000 nm pitch Ge NCN arrays. (Reprinted from ref. 31, Copyright 2013.)

simultaneously, with the absorption showing a strong diameter dependency.[16] The detailed relationship between the absorption of an NPL array and the NPL diameter and pitch has been explored with finite difference time domain (FDTD) simulations with Ge as the model material, as shown in Fig. 4b.[31] It can be seen that optimal NPL structures can be identified with the best absorption ∼80%.

To further enhance the broadband optical absorption capability, multi-diameter NPL (MNPL) structures have been studied, with smallest diameter tip for minimal reflectance and largest diameter base for maximal effective absorption coefficient.[16,31] Particularly, Fan *et al.* have presented ordered arrays of dual-diameter NPLs (DNPLs) with a small diameter tip and a large diameter base for an impressive absorption of ∼99% of the incident light over wavelength range $\lambda = 300$–900 nm with a thickness of only 2 μm.[16] Such a DNPL array was constructed *via* template assisted vapor–liquid–solid (VLS) growth, utilizing dual-diameter anodic alumina membrane (AAM) as the template, which was achieved by a multi-step anodization and etching process. Fig. 4c shows an up-side-down cross-sectional SEM image of a blank AAM (*i.e.*, before growth) with top and bottom pore diameters (D_1 and D_2) of ∼40 and 110 nm, respectively. After the subsequent VLS growth, highly ordered Ge DNPLs embedded in the aforementioned AAM with $D_1 \sim 60$ nm and $D_2 \sim 130$ nm are formed (Fig. 4c, inset). The experimental absorption spectra of the obtained Ge DNPL arrays with equal lengths of about 1 μm for the two segments (total length of 2 μm), together with single-diameter NPL arrays with diameter of 60 and 130 nm are plotted in Fig. 4d. The Ge DNPL array exhibits 95–100% absorption for $\lambda = 900$–300 nm, which is a drastic improvement over single-diameter NPLs (Fig. 4d).

In order to further understand light coupling, propagation and absorption in NPL arrays, Hua *et al.* carried out a more systematic investigation on the broadband solar spectrum absorption of MNPL arrays analyzed with FDTD simulations with Ge as the model material.[31] The schematic of the Ge MNPL arrays is shown in Fig. 4e, with the number of the segments $N = 3$. The lengths/height of the NPL arrays and the NCN (Nanocone) arrays here are all 2 μm. It was discovered that the broadband absorption of MNPLs approached that of NCNs when N increases, with $N = 7$ yielding the same light absorption level as NCNs, as demonstrated in Fig. 4f.

The above results have shown that by engineering the shape of nanopillars, their optical absorption can be greatly improved. On the other hand, the PV performance of nanopillar based solar cells can still be limited by their relatively large surface area compared to thin film solar cells. In this case, the choice of materials is crucial, that is, materials systems such as CdS, CdTe which have low surface recombination velocities are desirable as nanopillar materials.[2,11,60] What's more, although materials such as Si and GaAs have a high surface recombination velocity, decent device performance can also be achieved if proper surface passivation schemes can be applied.[64,65]

3.2 Nanocones, nanopyramids and nanodomes

3.2.1 Nanocones (NCNs). NCNs have been widely considered as the optimal structure for light absorption for solar cells because of their graded transition of effective refractive index between the nanostructure and air.[66–68] Zhu *et al.* reported the fabrication of vertical hydrogenated amorphous silicon (a-Si:H) NW and NCN arrays.[22] Fig. 5a–d show the schematic of the fabrication process of an a-Si:H nanostructure. Specifically, hot wire chemical vapor deposition (HWCVD) was utilized to grow a 1 μm thick a-Si:H film on an indium-tin-oxide (ITO) coated glass substrate (Fig. 5a). On top of the a-Si:H thin film, silica nanoparticles were packed into a single layer by the Langmuir–Blodgett method. These silica nanoparticles (Fig. 5b) served as an etch-mask in the reactive ion etching (RIE) process, considering that the etching rate of a-Si:H is much higher than that of silica. With different RIE conditions, either NWs (Fig. 5c) or NCNs (Fig. 5d) can be obtained.[69] Fig. 5e–g show the volume weighted effective refractive index profiles at the interface between air and an a-Si:H thin film (Fig. 5e), NW arrays (Fig. 5f), and NCN arrays (Fig. 5g). NCN arrays show the best refractive index transition from air to a-Si:H. Fig. 5h shows a photograph of three samples: 1 μm thick a-Si:H thin film (left), NW arrays (middle), and NCN arrays (right) with the same device thickness

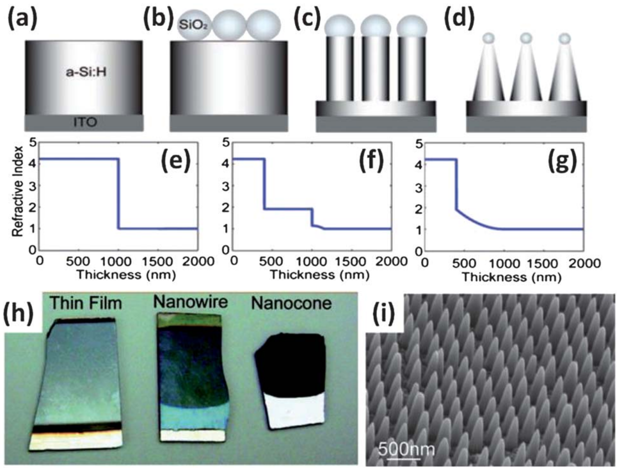

Fig. 5 (a) 1-μm thick a-Si:H on ITO coated glass. (b–d) SiO_2 nanoparticles on the a-Si:H (b) thin film, (c) NWs, (d) NCNs. (e–g) Volume-weighted effective refractive index profile at the interfaces between air and the a-Si:H (e) thin film, (f) 600 nm NWs, and (g) 600 nm NCNs. (h) Photographs of different a-Si:H solar cell samples: thin film (left), NW (middle) and NCN (right). (i) SEM image of a-Si:H NCNs. (Reprinted from ref. 22, Copyright 2009 American Chemical Society.)

with Fig. 5i showing the SEM of regular array of NCNs. It is obvious that NCNs greatly suppress reflection, and the absorption spectrum measurement showed that NCNs have a broadband and omnidirectional anti-reflection effect with absorption maintained above 93% between 400 and 650 nm.

Besides a-Si NCNs, crystalline-Si (c-Si) NCNs have also been fabricated.[27,70–72] It was found that c-Si NCNs can be combined with conductive polymer (PEDOT:PSS) to form hybrid solar cells, as shown in Fig. 6a.[32] In this work, it was demonstrated that the Schottky junction between the polymer and Si can extract photon-generated charge carriers effectively. Light scattering with c-Si NCNs increases the optical travel length of photons inside the material, thus giving rise to higher light absorption. It was found that when the aspect ratio of the nanocone (height/diameter of a nanocone) structure was less than two, both excellent antireflection and light scattering were obtained. As we can see from Fig. 6b, NCNs samples show higher absorption than planar ones. The light trapping effect that increases the optical path length becomes more prominent, especially when the substrate becomes thinner.

With growing interest in designing thin film silicon solar cells with an active layer thickness of several micrometers, it becomes more-and-more important to improve light absorption in silicon thin film for higher efficiency and lower cost. In this regard, Wang *et al.* introduced a double-sided NCN grating design (Fig. 6c) and optimized the front and back surfaces for antireflection and light trapping, respectively. The absorption of the optimized structure was found to be close to Yablonovitch limit (Fig. 6d).[27] In this work, NCNs were utilized as the basic building elements to form 2-D square lattices for the grating structure. Moreover, these researchers demonstrated that the double-sided strategy could be applied to a range of thicknesses, and suggested that the NCNs arrays could be obtained *via* Langmuir–Blodgett (LB) assembly method in conjunction with RIE.

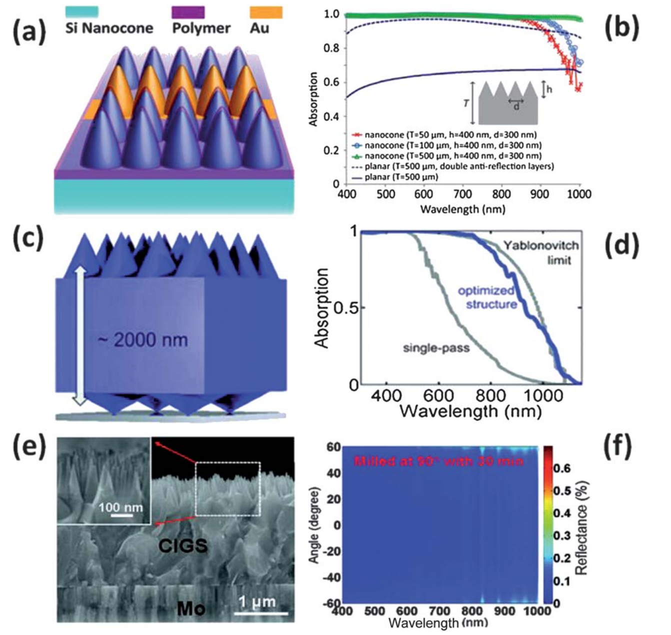

Fig. 6 (a) Schematic of a hybrid silicon nanocone–polymer solar cell. (b) Simulated absorption curves of Si substrates (thickness T = 50, 100, and 500 μm) with nanocones (diameter d = 300 nm, height h = 400 nm), planar Si substrate (thickness T = 500 μm) with double antireflection layers (100 nm thick SiO_2 followed by 60 nm thick Si_3N_4), and a planar Si (thickness T = 500 μm) substrate without any coating. (Reprinted from ref. 32, Copyright 2012 American Chemical Society.) (c) Double sided nanocone structure. (d) Absorption of the optimized double sided nanocone structure which is close to the Yablonovitch limit. (Reprinted from ref. 27, Copyright 2012 American Chemical Society.) (e) The cross-sectional SEM image of the CIGS thin film after ion milling at 90° for 30 min. (f) Reflection performance of the CIGS NTRs milled at 90° for 30 min. (Reprinted from ref. 73, Copyright 2011 American Chemical Society.)

Besides using Si, Liu *et al.* fabricated large area and uniform $Cu(In,Ga)Se_2$ nanotip arrays (CIGS NTRs) from CIGS thin films *via* direct sputtering of a CIGS target in conjunction with an Ar+ milling process.[73] NTRs are essentially NCNs with smaller dimensions. The researchers demonstrated a precise control over the length of CIGS NTRs and the tilting orientations by controlling the milling time and incident angles. The SEM image of the sample milled at 90° for 30 min from a CIGS thin film is shown in Fig. 6e. Here, uniform CIGS NTRs were formed on top of CIGS thin film. The obtained CIGS NTRs achieved a reflectance less than 0.1% for incident wavelengths from 300 nm to 1200 nm. To further characterize the antireflection properties, angular dependent reflectance mapping was performed on the CIGS NTRs at wavelengths from 400 to 1000 nm with milling at 90° for 30 min, as shown in Fig. 6f. The NTR CIGS solar cells demonstrated a 160% relative conversion efficiency improvement as compared to the planar counterparts.

3.2.2 Nanopyramids (NPMs). Akin to NCNs, NPMs are also tapered nanostructures but with square bases. Liang *et al.* demonstrated that GaAs thin film NPM arrays achieved enhanced absorption over a broad range of wavelengths and incident angles, even at large curvature bending.[74] The NPMs also provided as gradual a change of refractive index as the NCNs mentioned above. Han and Chen demonstrated

Si_3N_4/c-Si/SiO_2/Ag NPM structures which reached the Lambertian limit (Fig. 7a).[29] Intriguingly, they proved that the mirror symmetry of the NPM arrays should be broken in order to improve absorption, as illustrated in Fig. 7b. It was observed that at normal incidence the absorptance of the skewed pyramids even exceeded the Lambertian limit over a broad range of wavelengths, as illustrated in Fig. 7b. Mavrokefalos *et al.* demonstrated an inverted NPM scheme for crystal silicon thin films, which also performed a broadband absorption close to the Lambertian limit.[75]

3.2.3 Nanodomes (NDMs). Although the NCNs are superior structures for photon trapping, in certain thin film PV applications smoother structure are required for uniform film coating. In this regard, Deceglie *et al.* fabricated NDM structures as templates for the deposition of thin film n–i–p a-Si:H solar cells.[76] The calculated photo-carrier generation rate distributions of different device structures are shown in Fig. 8a–d. From Fig. 8b and d, it can be seen that with a NDM template of either aluminum doped zinc oxide (AZO) layer or Ag layer, the optical absorption in the a-Si:H layer is much higher than their planar counterpart in Fig. 8a. The absorption efficiency in the NDM parts of the a-Si:H layer is higher than other parts. In fact, even an ITO top layer with NDM configuration can help to enhance absorption of the planar a-Si:H thin film (Fig. 8c), to which could be attributed the "nanolens" effect. Ultimately, the energy conversion efficiency of an NDM structure based solar cell device with only a 200 nm thick a-Si:H layer is 7.25%, which is much larger than that of a flat device with the same thickness of a-Si:H and even superior to the efficiency of a planar sample with a 360 nm thick a-Si:H layer, as shown in Fig. 8e.

Moreover, Zhu *et al.* experimentally reported NDM a-Si:H solar cells formed by depositing thin films on a glass or quartz substrate with short NCNs.[77] The NDM solar cells consist of a 100-nm thick Ag layer as back reflector, an a-Si:H layer as the active part and 80 nm transparent conducting oxide (TCO) layers on both top and bottom of the active layer as electrodes, as shown in Fig. 8f. Fig. 8g shows the SEM image of a NDM solar cell device. The NCN template is fabricated by RIE with tunable diameter and spacing in the range of 100–1000 nm. With an NCN template of 100 nm base diameter, 450 nm spacing and 150 nm height, NDM a-Si:H solar cells can enhance the optical absorption significantly compared to flat control samples (Fig. 8h). The NDM configuration can not only reduce the reflection (which is the main reason for short wavelength light loss), but also breaks the interference effect for longer wavelengths, as discussed above.

Besides thin film solar cells, Ding *et al.* prepared novel solid-state dye-sensitized solar cells (ss-DSSCs) with plasmonic back reflectors consisting of 2D arrays of Ag NDMs.[78] The schematic of the device superstrate structure is shown in Fig. 8i. A hexagonally close-packed NDM-patterned template was embossed onto TiO_2 nanoparticles and an ethyl cellulose thin film to transfer the NDM pattern, and after treatment on TiO_2 thin films, the Ag electrode was fabricated by thermal evaporation. Fig. 8j shows the SEM image of imprinted TiO_2 thin films after sintering. The NDM-patterned Ag thin film not only acted as electrode and back reflector, but also enhanced light absorption through light scattering and surface plasmon polariton modes. Compared to the planar Ag electrode, this nanopatterned electrode can improve the short-circuit photocurrent (J_{sc}) by 16% with Z907 dye and 12% with C220 dye (Fig. 8k), respectively.

3.3 High aspect ratio tapered nanostructures

High aspect ratio tapered nanostructures, such as nanoneedles (NNs), nanospikes (NSPs), and nano-syringes,[17,73,79–82] possess an impressive photon management/trapping capability attributed to their strong light scattering, in addition to a gradual change of the effective refractive index from the top to the bottom.[83] Therefore, high aspect ratio tapered nanostructures have been extensively developed for efficient photon capturing. For example, Chueh *et al.* have explored the direct synthesis of black Ge based on crystalline/amorphous core/shell Ge NN arrays with ultrasharp tips (~4 nm) enabled by the Ni catalyzed vapor–solid–solid growth process.[79] An SEM image of a Ge NN array is shown in Fig. 9a, depicting the quasi-vertical orientation of the NNs arising from the steric interactions of the highly dense array, and the inset shows TEM of a single NN. Ge NN arrays exhibit a remarkable photon trapping capacity. Fig. 9b demonstrates the reflectance spectrum at normal incidence for Ge NN arrays with different lengths, as well as Ge NW arrays (~20 μm long) and a Ge thin film (TF) (~1 μm thick) substrate. It is clear that a drastic reduction of reflectance occurs for NN

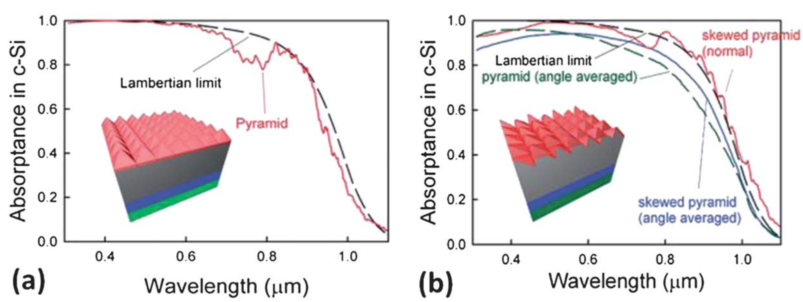

Fig. 7 (a) Absorption of pyramid nanostructure. Only the absorption in Si is accounted for. The height is 566 nm and the length of the base is 800 nm. (b) When symmetry is broken, absorption becomes better and even exceeds the Lambertian limit. The height of the skewed pyramid is 636 nm and the longer side of the base is 900 nm. (Reprinted from ref. 29, Copyright 2010 American Chemical Society.)

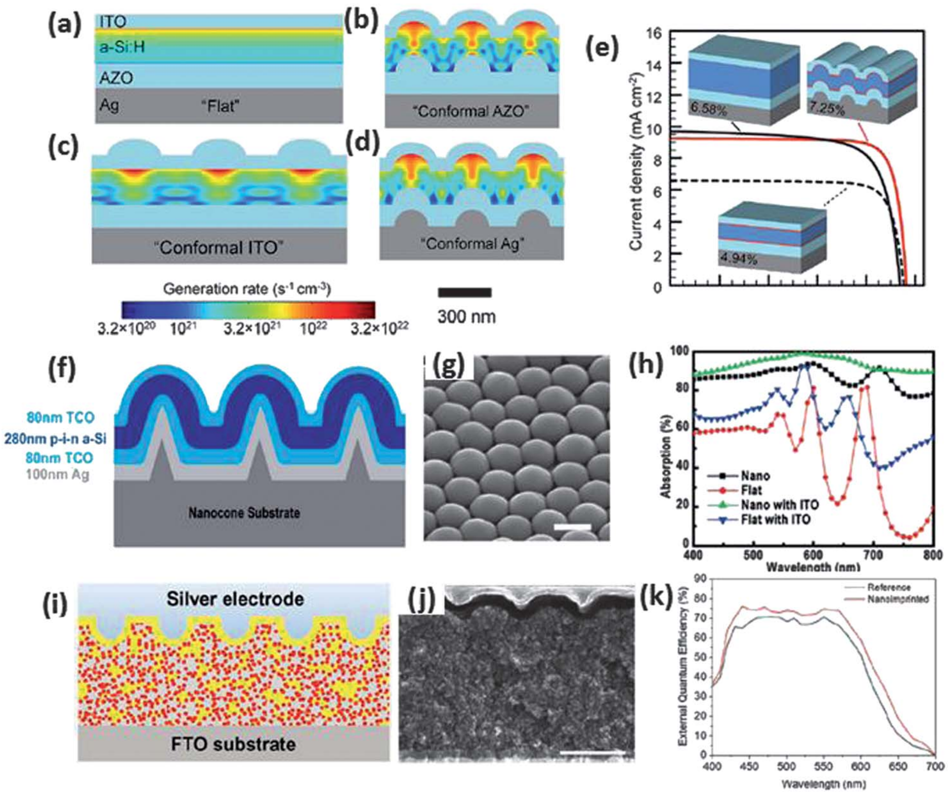

Fig. 8 (a–d) Schematics of different a-Si:H solar cell configurations. The thickness of ITO, a-Si:H, AZO and Ag layers are 80 nm, 200 nm, 130 nm, and 200 nm, respectively. Other parameters are introduced in this reference. (e) Current–voltage curves of different solar cell structures. (Reprinted from ref. 76, Copyright 2012 American Chemical Society.) (f) Schematic of nanodome solar cells. (g) SEM picture of a nanodome solar cell device. The scale bar is 500 nm. (h) Absorption curves of devices with normal incident light. (Reprinted from ref. 74, Copyright 2010 American Chemical Society.) (i) Schematic of plasmonic dye-sensitized solar cells with TiO_2 in grey, dye molecules in red, and spiro-OMeTAD in yellow. (j) 45-degree-tilted SEM picture of imprinted TiO_2 films after sintering. (k) External quantum efficiency (EQE) spectra of ss-DSSC using C220 dye. (Reprinted from ref. 77, Copyright 2011 WILEY-VCH Verlag GmbH & Co. KGaA, Weinheim.)

length >1 μm when comparing NNs to the TF. The NN arrays exhibit a reflectance of <1% for all wavelengths beyond this length. In contrast, Ge NWs with a much larger length of ~20 μm exhibited a reflectance of 2–10%, inferior to the NN arrays. The optical photograph of Ge TF, NW ($L \sim 20$ μm) and NN ($L \sim 1.1$ μm) substrates clearly illustrates the drastic reflectance suppression for NNs as compared to both NWs and TF (inset of Fig. 9b). The remarkably low reflectance of Ge NN arrays can be attributed to the cone-shaped features of the structures with ultra-sharp tips and their near vertical orientation arising from their high surface density as enabled by the Ni catalytic growth.

In addition, Yu *et al.* reported self-organized 3-D Al NSP arrays on thin Al foils *via* simple and scalable direct current anodization of Al substrates under high voltage in conjunction with wet chemical etching.[17] Thereafter, a-Si and CdTe thin films were conformally deposited on the NSP structures to form 3-D nanostructures with strong light absorption over a broad range of wavelengths and incident angles. Fig. 9c illustrates a 60° tilted-angle-view SEM image of NSP arrays coated with a 100 nm a-Si film. The inset is an image with higher magnification, showing the uniformity of the a-Si thin film deposited on Al NSPs.

The a-Si NSP arrays demonstrated high absorption with small dependence on angle and wavelength, with over 90% absorption over the entire angle range for 400–800 nm wavelength, as shown in Fig. 9d.

Moreover, taking advantage of the gradual change in effective refractive index of the high aspect ratio tapered nanostructures, Yeh *et al.* demonstrated ZnO nano-syringe arrays synthesized by the hydrothermal method as an effective antireflection coating to improve the optical absorption of GaAs-based solar cells.[80] Fig. 9e shows the cross-sectional SEM image of the ZnO nano-syringes, with an average nano-syringes length of 0.86 μm. The high-magnification image in the inset revealed that the nano-syringes are terminated with ultra-sharp tips. Taking advantage of the ZnO nano-syringes with favorable tip geometry, the abrupt interface between air and GaAs can be replaced with the engineered antireflection layers containing a smooth transition of refractive index, significantly suppressing the reflection of the device over a wide range of wavelengths. Fig. 9f shows UV-Vis reflectance spectra of the three GaAs solar cells with different surface conditions: that without any antireflection layers (bare), that only with $\lambda/4$ thick Si_3N_4, and that with ZnO nano-syringes/SiO_2/Si_3N_4. For the solar cell with an Si_3N_4 layer, the reflection reaches a minimum around 750 nm wavelength but gradually increases as the wavelength moves toward the UV region, functioning as a typical $\lambda/4$ AR coating. It is apparent that the addition of ZnO nano-syringes/SiO_2 to the Si_3N_4 layer leads to an even

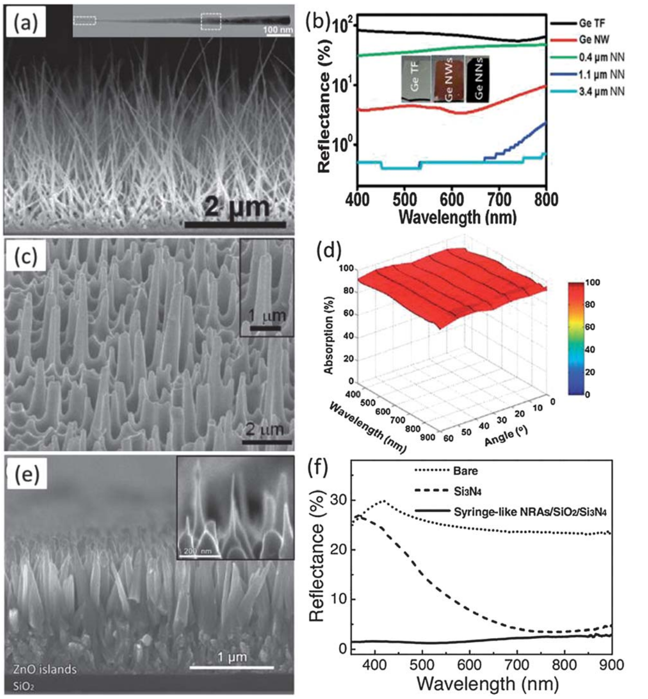

Fig. 9 (a) SEM image of Ge NN arrays grown on a Si/SiO_2 substrate. The inset shows TEM of a single NN. (b) The reflectance spectra of Ge TF, Ge NWs ($d \sim 30$ nm, $L \sim 20$ μm), and Ge NNs with different lengths. The inset shows the optical images of three representative substrates. (Reprinted from ref. 79, Copyright 2010 American Chemical Society.) (c) 60° tilted-angle-view SEM images of Al NSP arrays substrate deposited with a-Si. The inset shows a single Al NSP coated with a-Si. (d) Angular and wavelength dependent absorption spectra of 3-D Al NSP arrays deposited with 100 nm thick a-Si. (Reprinted from ref. 17, Copyright 2011 American Chemical Society.) (e) Cross-sectional SEM images of the ZnO nano-syringes. The inset is a high-magnification image showing the ultra-small tips on the ZnO nano-syringes. (f) Specular reflection measured on the GaAs solar cells with bare, Si_3N_4, and syringe like NRAs/SiO_2/Si_3N_4 surfaces. (Reprinted from ref. 80, Copyright 2011 WILEY-VCH Verlag GmbH & Co. KGaA, Weinheim.)

lower reflectance of below 3% for the entire range of wavelengths studied.

3.4 3-D nanoholes (NHLs) and nanowells (NWLs)

So far all the nanostructures for efficient photon management discussed above can be categorized as "positive" structures with respect to the substrates, that is, the structures protrude out from the substrates into free space. In fact, there are also some reports on photon trapping in deep "negative" nanostructures, for example, NHLs and NWLs.[15,84–86] In general, light trapping in the "positive" nanostructure arrays can be simply described as the result of photon multiple scattering within the nanostructures, which increases effective optical path length of a photon and absorption probability.[18,29] Nevertheless, structures such as NHLs and NWLs with cylindrical cavities provide geometric confinement for incoming photons naturally, thus the photon trapping process is expected to be different.[15] Specifically, Han and Chen investigated c-Si NHL arrays as light absorbing structures for PV devices and compare them to nanorod (NRD) arrays *via* simulation.[84] A schematic of the NHL arrays is illustrated in Fig. 10a, with that of NRD arrays in the inset. Fig. 10b shows the calculated absorption spectra for the NHL and the NRD array structures when the thickness d is 2.33 μm and 1.193 mm. The c-Si filling fraction and the lattice constant are 0.5 and 500 nm, respectively. In both cases, the NHL array demonstrates a higher absorption when λ is less than approximately 750 nm. When $d = 1.193$ mm, the NHL array has a slightly higher ultimate efficiency of 42.6% compared to 41.2% for the NRD array. However, when $d = 2.33$ μm, the efficiency is 27.7 and 24.0% for the NHL and the NRD array, respectively, giving a larger difference between the two structures. This implies that NHL arrays have a more efficient photon management than NRD arrays for practical thickness. In addition, it indicated that a NHL array structure with one-twelfth the c-Si mass and one-sixth the thickness of a standard 300 μm Si wafer have an equivalent ultimate efficiency. The strong optical absorption of NHL arrays is attributed to effective optical coupling of incident light into the arrays, as well as the existence of a large density of waveguide modes.

Besides simulation of the optical properties of c-Si NHL arrays, periodic photon NWLs were fabricated with a low-cost and scalable approach, followed by systematic investigation of their photon capturing properties combining experiments and simulations by Leung *et al.*[15] In this work, perfectly ordered flexible three-dimensional arrays of NWLs with greatly tunable pitch, diameter, and depth have been fabricated based on a self-organized approach. In order to understand the photon-trapping processes in regular NWL arrays, thin films of a light-absorbing material were conformally coated in the NWLs. Fig. 10c demonstrates cross-sectional SEM image of a 1 μm pitch NWL sample with diameter of 870 nm, showing a

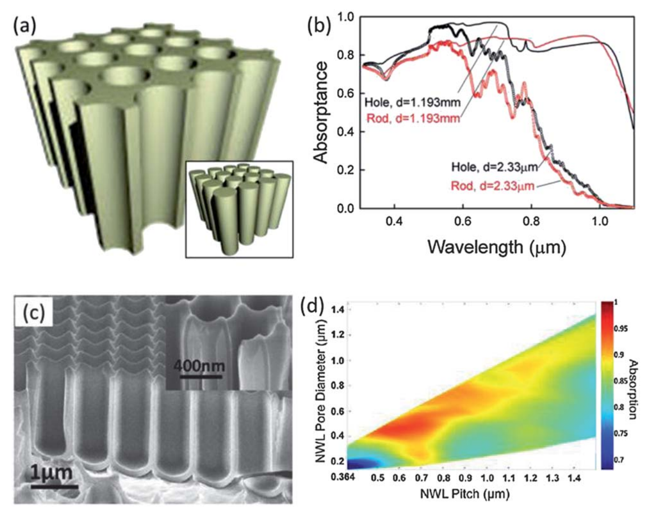

Fig. 10 (a) Schematic of NHL arrays, and that of NRD arrays in the inset. (b) Calculated absorption spectra for the NHL and the NRD array structures when the thickness d is 2.33 μm and 1.193 mm. (Reprinted from ref. 84, Copyright 2010 American Chemical Society.) (c) Cross-sectional SEM image of a 1 μm pitch NWL sample with a 50 nm a-Si conformal coating. The inset is a high-magnification SEM image showing a uniform a-Si coating on an NWL side wall. (d) The experimental 2D contours of the above-band gap absorption plotted as a function of NWL pore diameter and pitch. (Reprinted from ref. 15, Copyright 2012 American Chemical Society.)

conformal a-Si coating with low-pressure chemical vapor deposition. To understand comprehensively photon management in NWL arrays with different geometries, above-band gap broadband absorption for NWL arrays with pitches from 364 nm to 1.5 μm and different NWL diameters was obtained and plotted as a semi-2-D contour, shown in Fig. 10d. Intriguingly, it is found that a proper periodicity greatly facilitates photon capturing process in the NWLs, primarily owing to optical diffraction and resonance in NWLs. Meanwhile, the nanoengineered morphology provides the nanostructures with a broad-band, efficient light-absorption.

3.5 Hybrid nanostructures

Besides the aforementioned individual nanostructures, hybrid nanostructures for light management also attracted much attention. For example, Ho *et al.* demonstrated a hybrid structure consisting of SiO_2 NRDs and p-GaN microdomes for an InGaN-based multiple-quantum-well solar cell.[87] InGaN-based solar cells have direct and tunable band gaps, thus achieving a promising theoretical efficiency of over 40%.[88–90] However, the abrupt change of refractive index between air and the device leads to optical loss at the interface, which limits the practical efficiency. In this work, a microdome structure was fabricated to yield multiple photon scatterings in the structure. With an intermediate refractive index ($n \sim 1.56$) between air ($n \sim 1$) and GaN ($n \sim 2.5$), subwavelength SiO_2 NRD arrays (NRAs) can further reduce the surface reflection. The micro- and nano-scale hierarchical structures combined multiple reflections caused by the microdome morphology with the subwavelength feature of the NRDs.

In another work, Lin *et al.*[91] demonstrated an integrated-nanopillar–nanowell (i-NPW) array by integrating NPL and NWL arrays together vertically for 3-D thin film PV applications.

Fig. 11a illustrates a cross-sectional SEM image of 1 μm pitch i-NPW arrays with a 40 nm a-Si coating (left), and higher magnified images of different parts of the i-NPW structure (right), showing the conformal a-Si coating over the 3-D structures. Fig. 11b demonstrates the normal incident absorption spectra of samples on five different kinds of structures: i-NPWs, NPLs, NWLs, nanoconcaves (NCONs) and a planar substrate. Fig. 11c illustrates the simulated cross-sectional $|E|^2$ distribution on i-NPWs. The authors demonstrated that the integrated nanostructures combining both "positive" and "negative" nanostructures showed more efficient light absorption than the "positive" or "negative" nanostructures alone over a broad range of wavelengths and incident angles, as shown in Fig. 11d. Impressively, the 2 μm thick i-NPW arrays with only 40 nm amorphous silicon coating displayed a day-integrated absorption of about 89%, while for the planar control sample absorption was only about 33%.

3.6 Light management in nanospheres

Most of the aforementioned nanostructures are quasi-one-dimensional structures or variants of them. In fact, intriguing light management properties have also been discovered in nanospherical structures. Particularly, Yao *et al.* fabricated nanocrystalline-Si (nc-Si) nanospheres with silica nanospheres as templates.[36] After etching away silica nanospheres, closely packed hollow nc-Si nanospheres were formed as shown in Fig. 12a. Preliminary optical measurements showed the improvement of absorption with nanospheres over a planar control sample, as shown in Fig. 12b. Further study has revealed the existence of low quality factor (low-Q) whispering gallery modes in spherical nanoshells, shown in Fig. 12c.[36] Whispering gallery mode resonators with (low-Q) have high absorption, low

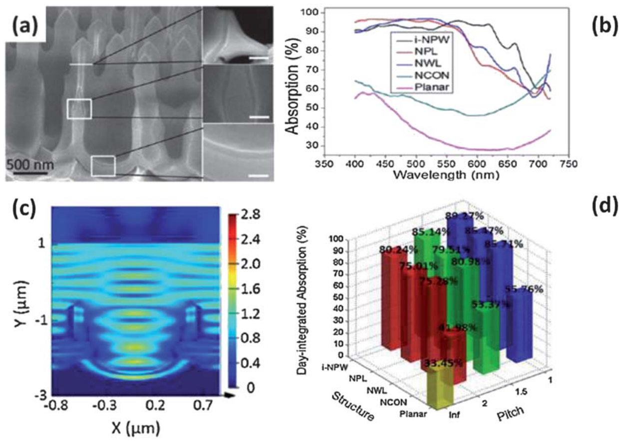

Fig. 11 (a) Cross-sectional SEM image of 1-μm pitch integrated nanopillar–nanowell (i-NPW) arrays with a 40 nm a-Si coating (right, the scale bar is 100 nm), and higher magnified SEM images of particular parts of the i-NPW structure (left). (b) The normal incident absorption spectra of the five samples: integrated i-NPW, nanopillar (NPL), nanowell (NWL), nanoconcave (NCON), planar. (c) Simulated cross-sectional $|E|^2$ distribution of the electromagnetic wave on i-NPWs. (d) Day-integrated solar energy absorption of all the five structures. (Reprinted from ref. 91, Copyright 2013 American Chemical Society.)

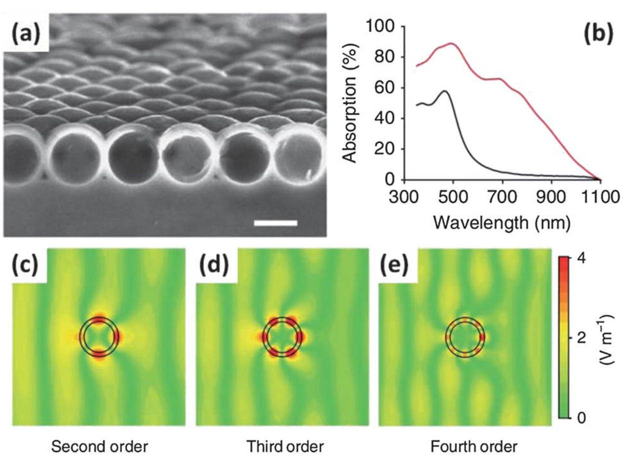

Fig. 12 (a) An SEM cross-sectional image of a single layer of Si spherical nanoshells on a quartz substrate. Scale bar is 300 nm. (b) Absorption spectra under normal incidence measured by integrating the sphere. Black line and red line are for flat sample and nanoshell sample, respectively. (c–e) Full-wave simulations of EM waves coupled with a single Si nanoshell. $|E|$ distribution of the first three modes with resonance wavelengths (c) 986, (d) 796 and (e) 685 nm, respectively. The E field is perpendicular to the paper plane with light amplitude of 1 V m^{-1} for all wavelengths. (Reprinted from ref. 36, Copyright 2012 American Chemical Society.)

frequency selectivity and high coupling efficiency. The light path in the active layer was enhanced because light was coupled into the resonant modes, as mentioned above. In parallel to this work, Grandidier *et al.* also studied the whispering gallery modes in dielectric nanospheres and demonstrated that light absorption can be significantly enhanced by a strong whispering gallery mode in a-Si thin film solar cells.[9]

3.7 Plasmonic nanoparticles

Nanoparticles, or quantum dots, are usually described as 0-D nanostructures with dimensions far below optical wavelength. However, recent studies on plasmonics have shown that these small objects can strongly localize the incident light/electromagnetic wave energy within their vicinity. With a proper supporting substrate, they can also excite propagating plasmon polaritons at the dielectric interface. These behaviors have been harnessed as unique photon management schemes to improve material light absorption and PV device performance.[92–99] As one of the pioneering works, Pillai *et al.* carried out surface plasmon enhanced silicon solar cells, which used silver particles to introduce a surface plasmon effect to the Si solar cells.[95] The Ag particles were deposited by thermal evaporation followed by annealing. Fig. 13a shows schematics of the two kinds of solar cell samples they used, 1.25 μm silicon-on-insulator (SOI) test cells and 300 μm thick Si solar cells. Different silver particle sizes from 10 nm to 18 nm were tried. Results showed that for both SOI test cells and 300 μm thick Si solar cells, the Ag nanoparticles can enhance the absorption and short circuit current significantly. The highest enhancement can be as high as sevenfold for 300 μm cells at $\lambda = 1200$ nm (Fig. 13c) and even as high as 16-fold for SOI solar cells at $\lambda = 1050$ nm (Fig. 13b). These results paved the way for utilizing metal nanoparticles to improve light absorption of thin-film solar cells by the plasmonic effect.

In addition to the application in traditional Si and thin-film solar cells, metal nanoparticles are also utilized in dye-sensitized solar cells (DSSC)[92,98] and organic solar cells.[99–102] Particularly, Brown *et al.* reported plasmonic DSSCs by using Au nanoparticles to enhance the light absorption efficiency *via* surface plasmon resonance.[92] The Au nanoparticles with a diameter of about 15 nm were coated with 3 nm thick SiO_2 shells so that they will not act as recombination centers to deteriorate device performance. The core–shell Au–SiO_2 nanoparticles are either incorporated into the paste before device fabrication, or spin coated onto the device. Fig. 12d shows a schematic of how Au–SiO_2 nanoparticles enhance the local electric field intensity. Fig. 12e shows a schematic of the plasmonic DSSC device structure with uniformly distributed Au–SiO_2 nanoparticles by incorporating the nanoparticles into TiO_2 paste. From the performance of an N719 sensitized liquid electrolyte based DSSC (Fig. 12f), it can be seen that nearly all the important parameters, including short current density, open circuit voltage, fill factor and efficiency are improved with Au–SiO_2 nanoparticles. The efficiency is nearly doubled over the control sample.

In another work, Hsiao *et al.* introduced Au nanoparticles with different sizes and shapes into polymer solar cells.[102] It is found that different gold nanoparticles, including gold nanospheres and nanorods with different aspect ratio, exhibit different forward light scattering and backward light scattering properties as long as they show different localized surface plasmon resonance behaviour. So, by combining the localized surface plasmon resonance effect and the forward light scattering effect, the light trapping efficiency of polymer solar cells can be enhanced, which is supported by current–voltage characteristics and external quantum efficiency spectra in this work.

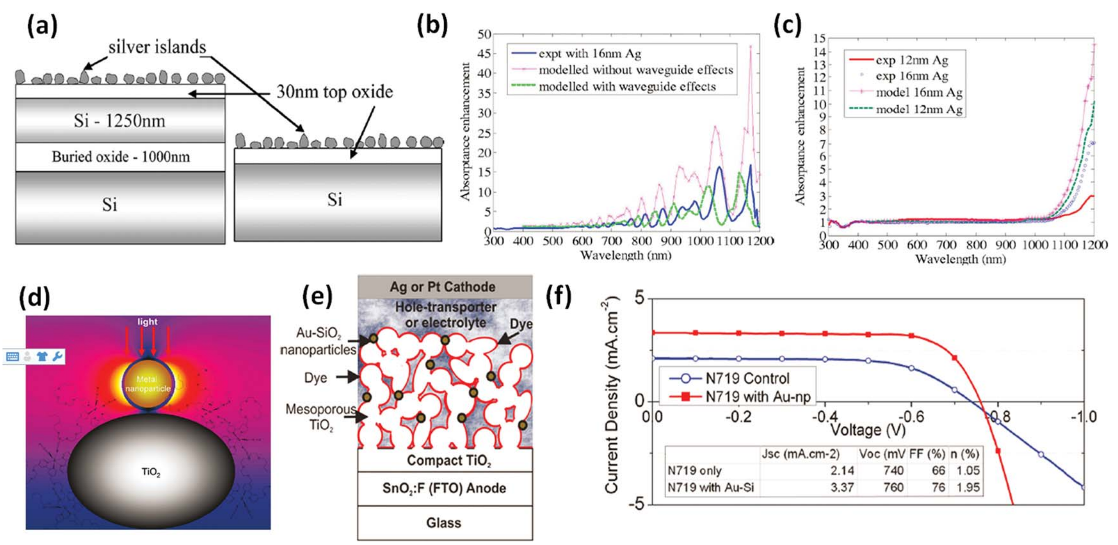

Fig. 13 (a) Schematic of silicon solar cells with Ag nanoparticles: left, silicon-on-insulator (SOI) with 1.25 μm active Si and right, wafer-based 300 μm planar Si cell. (b) Experimental and modeled result of photocurrent enhancement of SOI test solar cells. (c) Experimental and modeled result of photocurrent enhancement of 300 μm planar Si cells. (Reprinted from ref. 95, Copyright 2007 American Institute of Physics.) (d) Schematic of localized surface plasmon. (e) Schematic illustrations of DSSC incorporating core–shell Au–SiO_2 nanoparticles *via* putting the particles into the paste. (f) Current–voltage curves of N719 sensitized liquid electrolyte-based DSSC with and without Au–SiO_2 nanoparticles. Device thickness is 1.1 μm. (Reprinted from ref. 92, Copyright 2013 American Chemical Society.)

4 Summary and prospects

To implement a global terawatt-scale generation with PV technologies, further energy conversion efficiency improvement and cost reduction of solar panels with aggression are urgent. In this regard, developing novel low cost schemes to achieve efficient photon harvesting and photo-carrier collection is of paramount importance. Recent research has shown that engineered nanostructures have unique photon management capability, which may serve as one potential route leading to efficient PV devices. In this article, we have systematically reviewed photon management mechanisms in nanostructures, and provided a comprehensive summary of state-of-art research on several major categories of nanostructures with efficient light trapping properties. It was revealed that nanostructures with diverse configurations have their unique photon management properties, namely, tunable optical reflectance, transmittance and absorption. In addition, properly engineered nanophotonic structures have shown highly promising capability of harvesting sunlight over a broad range of wavelengths and incident angles. In our review, a variety of nanostructures, such as nanowires, nanopillars, nanopyramids, nanocones, nanospikes, and so forth, have been reviewed comprehensively with photonic materials including Si, Ge, CdS, CIGS, ZnO, *etc.* Moreover, the fabrication and optical property investigations of the aforementioned nanostructures have also been introduced. Overall, these nanostructures possess impressive efficient photon trapping capability by taking advantage of smooth gradient of effective refractive index, confining light in nanomaterials through waveguide mode, and/or localizing electromagnetic wave energy *via* plasmonic effects. These achievements have laid down a solid foundation for developing a new generation PV. Meanwhile, it is worth pointing out that an optimal PV device design has to incorporate the consideration of photocarrier dynamics which is sensitive to both material quality and device structure. A rational device design can be verified with modeling followed by experiments. Last but not the least, cost-effectiveness of a photon management scheme is the key for a practical application. A practical nanostructure fabrication process should be compatible with large scale production, such as a roll-to-roll process for thin film PV devices.

Acknowledgements

This work was partially supported by General Research Fund (612111) from Hong Kong Research Grant Council, National Research Foundation of Korea funded by the Korean Government (NRF-2010-220-D00060, 2008-0662256), HKUST Special Research Fund Initiative (SRFI11EG17).

References

1 M. Yu, Y. Long, B. Sun and Z. Fan, *Nanoscale*, 2012, **4**, 2783–2796.
2 R. Yu, Q. Lin, S. F. Leung and Z. Fan, *Nano Energy*, 2012, **1**, 57–72.
3 Y. Long, M. Yu, B. Sun, C. Gu and Z. Fan, *Chem. Soc. Rev.*, 2012, **41**, 4560–4580.
4 Z. Fan and A. Javey, *Nat. Mater.*, 2008, **7**, 835–836.
5 Z. Fan and J. C. Ho, *Int. J. Nanopart.*, 2011, **4**, 164–183.
6 Z. Y. Fan, H. Razavi, J. W. Do, A. Moriwaki, O. Ergen, Y. L. Chueh, P. W. Leu, J. C. Ho, T. Takahashi, L. A. Reichertz, S. Neale, K. Yu, M. Wu, J. W. Ager and A. Javey, *Nat. Mater.*, 2009, **8**, 648–653.
7 Z. Y. Fan, J. C. Ho, T. Takahashi, R. Yerushalmi, K. Takei, A. C. Ford, Y. L. Chueh and A. Javey, *Adv. Mater.*, 2009, **21**, 3730–3743.
8 Z. Y. Fan, J. C. Ho, Z. A. Jacobson, H. Razavi and A. Javey, *Proc. Natl. Acad. Sci. U. S. A.*, 2008, **105**, 11066–11070.
9 J. Grandidier, D. M. Callahan, J. N. Munday and H. A. Atwater, *Adv. Mater.*, 2011, **23**, 1272–1276.
10 J. Grandidier, R. A. Weitekamp, M. G. Deceglie, D. M. Callahan, C. Battaglia, C. R. Bukowsky, C. Ballif, R. H. Grubbs and H. A. Atwater, *Phys. Status Solidi A*, 2013, **210**, 255–260.
11 R. Kapadia, Z. Fan and A. Javey, *Appl. Phys. Lett.*, 2010, **96**, 103116.
12 Y. Qiu, S. Yang, H. Deng, L. Jin and W. Li, *J. Mater. Chem.*, 2010, **20**, 4439–4444.
13 Y. Sun, J. Sun, J. R. Long, P. Yang and C. J. Chang, *Chem. Sci.*, 2013, **4**, 118–124.
14 M. H. Lee, K. Takei, J. Zhang, R. Kapadia, M. Zheng, Y. Chen, J. Nah, T. S. Matthews, Y. Chueh and J. W. Ager, *Angew. Chem., Int. Ed.*, 2012, **51**, 10760–10764.
15 S. F. Leung, M. Yu, Q. Lin, K. Kwon, K. L. Ching, L. Gu, K. Yu and Z. Fan, *Nano Lett.*, 2012, **12**, 3682–3689.
16 Z. Y. Fan, R. Kapadia, P. W. Leu, X. B. Zhang, Y. L. Chueh, K. Takei, K. Yu, A. Jamshidi, A. A. Rathore, D. J. Ruebusch, M. Wu and A. Javey, *Nano Lett.*, 2010, **10**, 3823–3827.
17 R. Yu, K. Ching, Q. Lin, S. Leung, D. Arcrossito and Z. Fan, *ACS Nano*, 2011, **5**, 9291–9298.
18 C. Battaglia, C.-M. Hsu, K. Söderström, J. Escarré, F.-J. Haug, M. Charrière, M. Boccard, M. Despeisse, D. T. L. Alexander, M. Cantoni, Y. Cui and C. Ballif, *ACS Nano*, 2012, **6**, 2790–2797.
19 L. Hu and G. Chen, *Nano Lett.*, 2007, **7**, 3249–3252.
20 M. D. Kelzenberg, S. W. Boettcher, J. A. Petykiewicz, D. B. Turner-Evans, M. C. Putnam, E. L. Warren, J. M. Spurgeon, R. M. Briggs, N. S. Lewis and H. A. Atwater, *Nat. Mater.*, 2010, **9**, 239–244.
21 C. Lin and M. L. Povinelli, *Opt. Express*, 2009, **17**, 19371–19381.
22 J. Zhu, Z. F. Yu, G. F. Burkhard, C. M. Hsu, S. T. Connor, Y. Q. Xu, Q. Wang, M. McGehee, S. H. Fan and Y. Cui, *Nano Lett.*, 2009, **9**, 279–282.
23 Z. Yu, A. Raman and S. Fan, *Opt. Express*, 2010, **18**, A366–A380.
24 Z. Yu, A. Raman and S. Fan, *Proc. Natl. Acad. Sci. U. S. A.*, 2010, **107**, 17491–17496.
25 M. A. Green, *Progr. Photovolt.: Res. Appl.*, 2002, **10**, 235–241.
26 E. Yablonovitch and G. D. Cody, *IEEE Trans. Electron Devices*, 1982, **29**, 300–305.

27 K. X. Wang, Z. Yu, V. Liu, Y. Cui and S. Fan, *Nano Lett.*, 2012, **12**, 1616–1619.
28 E. Yablonovitch, *J. Opt. Soc. Am.*, 1982, **72**, 899–907.
29 S. E. Han and G. Chen, *Nano Lett.*, 2010, **10**, 4692–4696.
30 E. Yu and J. Van De Lagemaat, *MRS Bull.*, 2011, **36**, 424–428.
31 B. Hua, B. Wang, P. W. Leu and Z. Y. Fan, *Nano Energy*, 2013, DOI: 10.1016/j.nanoen.2013.03.016.
32 S. Jeong, E. C. Garnett, S. Wang, Z. Yu, S. Fan, M. L. Brongersma, M. D. McGehee and Y. Cui, *Nano Lett.*, 2012, **12**, 2971–2976.
33 L. Y. Cao, J. S. White, J. S. Park, J. A. Schuller, B. M. Clemens and M. L. Brongersma, *Nat. Mater.*, 2009, **8**, 643–647.
34 L. Cao, P. Fan and M. L. Brongersma, *Nano Lett.*, 2011, **11**, 1463–1468.
35 Y. Yu and L. Cao, *Opt. Express*, 2012, **20**, 13847–13856.
36 Y. Yao, J. Yao, V. K. Narasimhan, Z. Ruan, C. Xie, S. H. Fan and Y. Cui, *Nat. Commun.*, 2012, **3**, 664–670.
37 X. Meng, V. Depauw, G. Gomard, O. El Daif, C. Trompoukis, E. Drouard, C. Jamois, A. Fave, F. Dross and I. Gordon, *Opt. Express*, 2012, **20**, A465–A475.
38 D. Ko, J. R. Tumbleston, L. Zhang, S. Williams, J. M. DeSimone, R. Lopez and E. T. Samulski, *Nano Lett.*, 2009, **9**, 2742–2746.
39 A. Mihi, C. Zhang and P. V. Braun, *Angew. Chem.*, 2011, **123**, 5830–5833.
40 A. Chutinan, N. P. Kherani and S. Zukotynski, *Opt. Express*, 2009, **17**, 8871–8878.
41 G. Gomard, X. Meng, E. Drouard, K. El Hajjam, E. Gerelli, R. Peretti, A. Fave, R. Orobtchouk, M. Lemiti and C. Seassal, *J. Opt.*, 2012, **14**, 024011.
42 J. A. Schuller, E. S. Barnard, W. Cai, Y. C. Jun, J. S. White and M. L. Brongersma, *Nat. Mater.*, 2010, **9**, 193–204.
43 S. A. Maier, *Plasmonics: Fundamentals and Applications*, Springer, 2007.
44 E. Ozbay, *Science*, 2006, **311**, 189–193.
45 H. A. Atwater and A. Polman, *Nat. Mater.*, 2010, **9**, 205–213.
46 E. C. Garnett and P. D. Yang, *Nano Lett.*, 2010, **10**, 1082–1087.
47 K. Seo, M. Wober, P. Steinvurzel, E. Schonbrun, Y. Dan, T. Ellenbogen and K. B. Crozier, *Nano Lett.*, 2011, **11**, 1851–1856.
48 L. Cao, P. Fan, E. S. Barnard, A. M. Brown and M. L. Brongersma, *Nano Lett.*, 2010, **10**, 2649–2654.
49 P. M. Wu, N. Anttu, H. Xu, L. Samuelson and M. E. Pistol, *Nano Lett.*, 2012, **12**, 1990–1995.
50 S. L. Diedenhofen, O. T. Janssen, G. Grzela, E. P. Bakkers and J. Gómez Rivas, *ACS Nano*, 2011, **5**, 2316.
51 M. Law, L. E. Greene, J. C. Johnson, R. Saykally and P. D. Yang, *Nat. Mater.*, 2005, **4**, 455–459.
52 E. C. Garnett, M. L. Brongersma, Y. Cui and M. D. McGehee, *Annu. Rev. Mater. Res.*, 2011, **41**, 269–295.
53 B. Z. Tian, X. L. Zheng, T. J. Kempa, Y. Fang, N. F. Yu, G. H. Yu, J. L. Huang and C. M. Lieber, *Nature*, 2007, **449**, 885–889.
54 J. Tang, Z. Huo, S. Brittman, H. Gao and P. Yang, *Nat. Nanotechnol.*, 2011, **6**, 568–572.
55 S. Tsai, H. Chang, H. Wang, S. Chen, C. Lin, S. Chen, Y. Chueh and J. He, *ACS Nano*, 2011, **5**, 9501–9510.
56 J. Li, H. Yu, S. M. Wong, X. Li, G. Zhang, P. G. Lo and D. Kwong, *Appl. Phys. Lett.*, 2009, **95**, 243113.
57 B. Wang and P. W. Leu, *Opt. Lett.*, 2012, **37**, 3756–3758.
58 L. Cao, P. Fan, A. P. Vasudev, J. S. White, Z. Yu, W. Cai, J. A. Schuller, S. Fan and M. L. Brongersma, *Nano Lett.*, 2010, **10**, 439–445.
59 O. Ergen, D. J. Ruebusch, H. Fang, A. A. Rathore, R. Kapadia, Z. Fan, K. Takei, A. Jamshidi, M. Wu and A. Javey, *J. Am. Chem. Soc.*, 2010, **132**, 13972–13974.
60 Z. Fan, D. J. Ruebusch, A. A. Rathore, R. Kapadia, O. Ergen, P. W. Leu and A. Javey, *Nano Res.*, 2009, **2**, 829–843.
61 K. Cho, D. J. Ruebusch, M. H. Lee, J. H. Moon, A. C. Ford, R. Kapadia, K. Takei, O. Ergen and A. Javey, *Appl. Phys. Lett.*, 2011, **98**, 203101.
62 C. Ho, G. Lin, P. Fu, C. Lin, P. Yang, I. Chan, K. Lai and J. He, *Sol. Energy Mater. Sol. Cells*, 2012, **103**, 194–198.
63 H. Wang, K. Tsai, K. Lai, T. Wei, Y. Wang and J. He, *Opt. Express*, 2011, **20**, A94–A103.
64 D. R. Kim, C. H. Lee, P. M. Rao, I. S. Cho and X. L. Zheng, *Nano Lett.*, 2011, **11**, 2704.
65 M. D. Kelzenberg, D. B. Turner-Evans, M. C. Putnam, S. W. Boettcher, R. M. Briggs, J. Y. Baek, N. S. Lewis and H. A. Atwater, *Energy Environ. Sci.*, 2011, **4**, 866–871.
66 Y. Lu and A. Lal, *Nano Lett.*, 2010, **10**, 4651–4656.
67 S. Jeong, M. T. McDowell and Y. Cui, *ACS Nano*, 2011, **5**, 5800–5807.
68 J. Jung, Z. Guo, S. Jee, H. Um, K. Park and J. Lee, *Opt. Express*, 2010, **18**, A286–A292.
69 C. Hsu, S. T. Connor, M. X. Tang and Y. Cui, *Appl. Phys. Lett.*, 2008, **93**, 133109.
70 M. Dawood, T. Liew, P. Lianto, M. Hong, S. Tripathy, J. Thong and W. Choi, *Nanotechnology*, 2010, **21**, 205305.
71 B. Wang and P. W. Leu, *Nanotechnology*, 2012, **23**, 194003.
72 Y. Wang, N. Lu, H. Xu, G. Shi, M. Xu, X. Lin, H. Li, W. Wang, D. Qi and Y. Lu, *Nano Res.*, 2010, **3**, 520–527.
73 C. H. Liu, C. H. Chen, S. Y. Chen, Y. T. Yen, W. C. Kuo, J. Y. Juang, Y. K. Liao, H. C. Kuo, C. H. Lai and L. J. Chen, *Nano Lett.*, 2011, **11**, 4443–4448.
74 D. Liang, Y. Huo, Y. Kang, K. X. Wang, A. Gu, M. Tan, Z. Yu, S. Li, J. Jia and X. Bao, *Adv. Energy Mater.*, 2012, **2**, 1254–1260.
75 A. Mavrokefalos, S. E. Han, S. Yerci, M. S. Branham and G. Chen, *Nano Lett.*, 2012, **12**, 2792–2796.
76 M. G. Deceglie, V. E. Ferry, A. P. Alivisatos and H. A. Atwater, *Nano Lett.*, 2012, **12**, 2894–2900.
77 J. Zhu, C. Hsu, Z. Yu, S. Fan and Y. Cui, *Nano Lett.*, 2010, **10**, 1979–1984.
78 I. Ding, J. Zhu, W. Cai, S. Moon, N. Cai, P. Wang, S. M. Zakeeruddin, M. Grätzel, M. L. Brongersma and Y. Cui, *Adv. Energy Mater.*, 2011, **1**, 52–57.
79 Y. L. Chueh, Z. Y. Fan, K. Takei, H. Ko, R. Kapdia, A. Rathore, N. Miller, K. Yu, M. Wu, E. E. Haller and A. Javey, *Nano Lett.*, 2010, **10**, 520–523.
80 L. K. Yeh, K. Y. Lai, G. J. Lin, P. H. Fu, H. C. Chang, C. A. Lin and J. H. He, *Adv. Energy Mater.*, 2011, **1**, 506–510.

81 G. Lin, K. Lai, C. Lin and J. He, *Opt. Lett.*, 2011, **37**, 61–63.
82 Y. Chao, C. Chen, C. Lin and J. He, *Energy Environ. Sci.*, 2011, **4**, 3436–3441.
83 S. Jeong, S. Wang and Y. Cui, *J. Vac. Sci. Technol., A*, 2012, **30**, 060801.
84 S. E. Han and G. Chen, *Nano Lett.*, 2010, **10**, 1012–1015.
85 K. Peng, X. Wang, L. Li, X. Wu and S. Lee, *J. Am. Chem. Soc.*, 2010, **132**, 6872–6873.
86 A. Boukai, P. Haney, A. Katzenmeyer, G. M. Gallatin, A. A. Talin and P. Yang, *Chem. Phys. Lett.*, 2011, **501**, 153–158.
87 C. Ho, D. Lien, H. Chang, C. Lin, C. Kang, M. Hsing, K. Lai and J. He, *Nanoscale*, 2012, **4**, 7346–7349.
88 J. Wu, W. Walukiewicz, K. Yu, J. W. Ager, E. Haller, H. Lu and W. J. Schaff, *Appl. Phys. Lett.*, 2002, **80**, 4741–4743.
89 R. Dahal, B. Pantha, J. Li, J. Lin and H. Jiang, *Appl. Phys. Lett.*, 2009, **94**, 063505.
90 K. Lai, G. Lin, Y. Lai, Y. Chen and J. He, *Appl. Phys. Lett.*, 2010, **96**, 081103.
91 Q. Lin, B. Hua, S. Leung, X. Duan and Z. Fan, *ACS Nano*, 2013, **7**, 2725–2732.
92 M. D. Brown, T. Suteewong, R. S. S. Kumar, V. D'Innocenzo, A. Petrozza, M. M. Lee, U. Wiesner and H. J. Snaith, *Nano Lett.*, 2011, **11**, 438.
93 N. Kalfagiannis, P. G. Karagiannidis, C. Pitsalidis, N. T. Panagiotopoulos, C. Gravalidis, S. Kassavetis, P. Patsalas and S. Logothetidis, *Sol. Energy Mater. Sol. Cells*, 2012, **104**, 165–174.
94 H. Tan, R. Santbergen, A. H. M. Smets and M. Zeman, *Nano Lett.*, 2012, **12**, 4070–4076.
95 S. Pillai, K. Catchpole, T. Trupke and M. Green, *J. Appl. Phys.*, 2007, **101**, 093105.
96 K. Nakayama, K. Tanabe and H. A. Atwater, *Appl. Phys. Lett.*, 2008, **93**, 121904.
97 D. Derkacs, S. Lim, P. Matheu, W. Mar and E. Yu, *Appl. Phys. Lett.*, 2006, **89**, 093103.
98 C. Hagglund, M. Zach and B. Kasemo, *Appl. Phys. Lett.*, 2008, **92**, 013113.
99 S. Kim, S. Na, J. Jo, D. Kim and Y. Nah, *Appl. Phys. Lett.*, 2008, **93**, 073307.
100 C. Kim, S. Cha, S. C. Kim, M. Song, J. Lee, W. S. Shin, S. Moon, J. H. Bahng, N. A. Kotov and S. Jin, *ACS Nano*, 2011, **5**, 3319–3325.
101 J. Wu, F. Chen, Y. Hsiao, F. Chien, P. Chen, C. Kuo, M. H. Huang and C. Hsu, *ACS Nano*, 2011, **5**, 959–967.
102 Y. Hsiao, S. Charan, F. Wu, F. Chien, C. Chu, P. Chen and F. Chen, *J. Phys. Chem. C*, 2012, **116**, 20731–20737.

